Graph Cut-based Automatic Segmentation of Lung Nodules using Shape, Intensity, and Spatial Features

Xujiong Ye, Gareth Beddoe and Greg Slabaugh

Medicsight PLC, London, UK

Abstract. This paper presents a new, fully automatic method of accurately extracting lesions from CT data. It first determines, at each voxel, a five-dimensional feature vector that contains intensity, shape index, and 3D spatial location. Then, non-parametric mean shift clustering is applied to produce intensity and shape mode maps. Finally, a graph cut algorithm segments the image using a novel energy formulation that incorporates shape, intensity, and spatial features. A key difference from the usual graph construction is that we connect modes (small regions, or super-pixels resulting from mean shift clustering) instead of pixels. The initial foreground and background can be automatically obtained by calculating highly spherical regions based on the shape index map. The proposed method has been evaluated on a clinical dataset of thoracic CT scans that contains 100 nodules. A volume overlap ratio between each segmented nodule and the ground truth annotation is calculated. Using the proposed method, the mean overlap ratio over all the nodules is 0.81. On visual inspection as well as using a quantitative evaluation, the experimental results demonstrate the potential of the proposed method. The rich information provided by the joint spatial–intensity-shape features provides a powerful cue for successful segmentation of nodules adjacent to structures of similar intensity but different shape.

1 Introduction

Accurate and automatic segmentation of medical images is an essential component of a computer-aided diagnosis (CADx) system. However, medical image segmentation is typically a difficult task due to noise resulting from the image acquisition process, as well as the characteristics of the object itself and its neighborhood. Lesions may be embedded in areas of complicated anatomy; and may have very similar intensities to their adjacent tissues (e.g. juxta-vascular nodules). In such cases, traditional intensity-based or model-based methods may fail to properly segment the object [1-3]. For example, a contrast-based region growing approach was introduced in [1]. This method assumes that the region of interest appears as a bright or dark object relative to the surrounding tissue. However, since adjacent blood vessels have a similar intensity to the nodule, the segmentation tends to include a part of a blood vessel along with the nodule. A morphological approach was presented in [2]. One issue with this method is its sensitivity to the morphology template size, which makes it difficult to choose a suitable template for all different kinds of nodules. As indicated by the authors, this algorithm is targeted for small and high contrast nodules; thus for a large nodules, especially when a blood vessel is attached to a nodule, the algorithm might fail to properly delineate the nodule.

Image segmentation methods based on energy minimization have been intensively researched [4-10]. In particular, graph cut based methods, which can achieve a global minimum of energy functions used in image segmentation, have been shown much promise in medical image computing. However, in most graph-based methods, the graph vertices are constructed at image pixels, and the segmentation energy is composed of intensity terms. For example, Zheng *et al.* [5] proposed a framework to simultaneously segment and register the lungs and nodules in CT data. For segmentation, a 2D pixel based graph cut algorithm was applied on the 3D lung and nodule datasets. It is noted that, by representing a graph vertex using an image pixel, the number of nodes in the graph increases polynomically with the image size (N^D, where N is the number pixels in one of the D dimensions); this dramatically increases the computation time. To improve efficiency, Li *et al.* [6] introduced a graph built on a pre-segmentated image using a watershed algorithm. However, their graph cut formulation is solely based on the image intensities. It is known that pixel intensity can be locally erroneous due to noise and other image acquisition issues (such as Partial Volume Effect (PVE) in CT). Thus, in these cases, noise can adversely affect the performance of a graph-based segmentation. Slabaugh *et al*. [7] incorporated an elliptical shape prior into the graph-cut segmentation framework. Xu *et al*. [8] presented a graph-cuts based active contours approach to object segmentation method. Zheng *et al*. [9] constructed a graph Laplacian matrix for the estimation of Ground-Glass Opacity (GGO) nodule in CT. Recently, Liu *et al*. [10] applied ordering constraints into an energy smoothness term based on an initial labeling. A simple geometric shape prior was also incorporated in a graph cut segmentation.

In this paper, we propose an automatic mode-based graph cut method for lung nodule segmentation. An overview of the approach appears in Fig. 1. At each voxel in the image, the volumetric shape index (SI) is computed. The shape index, along with the image intensity and spatial position (x, y, z) are concatenated into a five dimensional feature vector at each voxel. In this five dimensional joint spatial-intensity-shape (JSIS) feature space, mean shift clustering is applied, producing intensity and shape index mode maps (super-pixels). Then, a graph is constructed using the super-pixels as vertices. Weights in the graph are computed using a novel energy formulation that considers not only image intensity but also the shape feature. The use of mean-shift generated super-pixels produces better results and improves speed significantly compared to a dense graph with vertices at every voxel. The experimental results on CT lung nodules demonstrate the high performance of the proposed method.

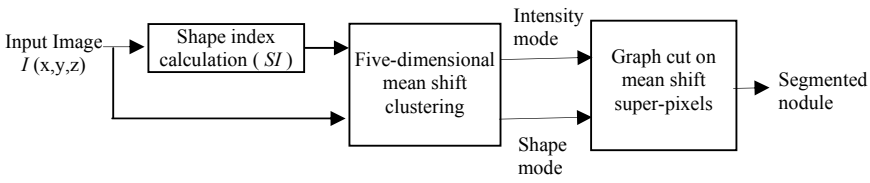

Fig. 1. Flow diagram of the proposed graph cut based method

2 Mean Shift Clustering of JSIS features

Our approach first computes the JSIS features, which are then clustered in a five-dimensional space using mean shift. In this section, we review the shape index feature and our mean shift approach.

2.1 Volumetric shape index: a 3D geometric feature

The volumetric shape index (SI) at voxel $p(x, y, z)$ can be defined as [11][12]:

$$SI(p) = \frac{1}{2} - \frac{1}{\pi} \arctan \frac{k_1(p) + k_2(p)}{k_1(p) - k_2(p)} \quad (1)$$

where $k_1(p)$ and $k_2(p)$ are the principal curvatures at voxel *p*, which are defined as:

$$k_1(p) = H(p) + \sqrt{H^2(p) - K(p)}, \quad k_2(p) = H(p) - \sqrt{H^2(p) - K(p)}$$

where $K(p)$ and $H(p)$ are the Gaussian and mean curvatures, respectively.

The calculation of the Gaussian and mean curvatures are based on the first and second fundamental forms of differential geometry. A practical approach for computing these forms is to use the smoothed first and second partial derivatives the image with respect to x, y, z as suggested in [13]. In this paper, prior to shape index calculation, a single-scale Gaussian smoothing is employed to obtain the smoothed image with standard deviation of 1.5.

Shape index represents the local shape feature at each voxel. Every distinct shape, except for the plane, corresponds to a unique shape index. For example, the shape index value of 1.00 indicates a sphere-like shape (e.g. nodule), and 0.75 indicates a cylinder-like shape (e.g. vessel). Based on the definition, volumetric shape index directly characterizes the topological shape of an iso-surface in the vicinity of each voxel without explicitly calculating the iso-surface. This feature provides rich information for automated segmentation of anatomical structures or lesions in medical images, where the region of interest is within an area of complicated anatomy and image intensities of different shapes are similar to each other (such as an adjoining lung nodule).

2.2 Combination of shape index feature into mean shift framework

For each voxel, 3D spatial location, intensity and volumetric shape index features are concatenated in the joint spatial-intensity-shape (JSIS) domain of dimension *d*=5. Given *n* data points p_i, *i*=1,…,*n* in a 5-dimensional space, the multivariate kernel is defined as the product of three radially symmetric kernels:

$$K_{h_s,h_r,h_{si}}(f) = c_{k,5} k\left(\left\|\frac{f^s}{h_s}\right\|^2\right) \cdot k\left(\left\|\frac{f^r}{h_r}\right\|^2\right) \cdot k\left(\left\|\frac{f^{si}}{h_{si}}\right\|^2\right) \quad (2)$$

where $c_{k,5}$ is a normalization constant which assures *K(f)* integrates to 1. f^s is the spatial location, f^r is the intensity and f^{si} is the shape index feature; h_s, h_r and h_{si} are the kernel window size for spatial, intensity and shape index kernel function. The normal kernel is used in this paper, where $k(f) = (2\pi)^{-d/2} \exp\left(-1/2\|f\|^2\right)$.

By using the mean shift framework [14], the shape index feature can be combined with the intensity for clustering. The mean shift vector with three kernel windows (spatial, intensity and shape index) can then be calculated as:

$$m_{h_s h_r h_{si}}(p_i) = \frac{\sum_{i=1}^{n} x_i g\left(\left\|\frac{f^s}{h_s}\right\|^2\right) \cdot g\left(\left\|\frac{f^r}{h_r}\right\|^2\right) \cdot g\left(\left\|\frac{f^{si}}{h_{si}}\right\|^2\right)}{\sum_{i=1}^{n} g\left(\left\|\frac{f^s}{h_s}\right\|^2\right) \cdot g\left(\left\|\frac{f^r}{h_r}\right\|^2\right) \cdot g\left(\left\|\frac{f^{si}}{h_{si}}\right\|^2\right)} - p_i \quad (3)$$

where $g(f) = -k'(f)$. The mean shift vector always points toward the direction of the maximum increase in the density function.

It is noted that the mean shift algorithm estimates the modes (the densest regions) of the multivariate distribution underlying the feature space. The set of points that converge to the same mode is defined as the attraction basin. Mean shift maps all the data samples to the local maxima of their corresponding attraction basin based on five-dimensional features. Super-pixels (modes) are formed for the set of pixels in each attraction basin. Each super-pixel has a constant shape index and intensity. This produces mode maps, namely an intensity mode map (M_I), and a shape index mode map (M_{SI}), and a spatial mode map (M_S). The spatial mode map is not used directly in our energy function; however, spatial information is utilized when defining neighbors in our graph. Fig. 2 shows a nodule attached to a vessel and its corresponding intensity and shape index mode maps. It can be noted that the mode maps ((c) and (d)) from JSIS mean shift clustering can be seen as "filtered" images and are less contaminated by outliers. In the following section, graph cut based segmentation is applied on these super-pixels.

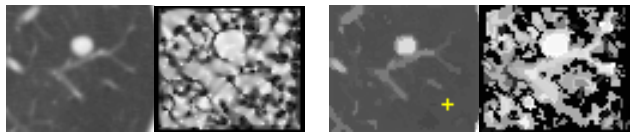

(a) (b) (c) (d)

Fig.2. One attached nodule with its intensity and shape mode maps (a) Original CT sub-image; (b) Shape index map based on Eq. (1); (c) Intensity mode and (d) shape index mode maps.

3 Automatic Graph Cut based Segmentation on Mean Shift Mode Map with Shape Feature

In this section, we consider the mode map as a graph *G*. As mentioned above, the graph *G*=(*V*, *E*) is defined with vertices $v \in V$ representing super-pixels determined

from five dimensional mean-shift clustering, and edges $\varepsilon \in E$ connecting adjacent super-pixels. A key difference from the usual graph construction is that we connect super-pixels instead of the original pixels. As a result, the number of vertices in *G* is greatly reduced compared to the original number of pixels in the image. Two key issues are addressed in the following two sub-sections: initialization and energy function definition.

3.1 Initialization based on high spherical concentration

In our previous work, we have developed an automatic lung nodule detection algorithm [15], which produced a small number of potential nodule regions. The aim of this paper is to accurately delineate each nodule boundary. Given that a nodule is generally either spherical or has local spherical elements, while a blood vessel is usually oblong, for each potential nodule region (or region of interest), a spherical concentration is calculated for the automatic estimation of initial nodule (foreground) region.

A cluster of high shape index voxels is automatically determined using hysteresis thresholding [13] applied to the shape index map. This algorithm finds a spherical region $\Re_s$ formed of 3D connected voxels that all have shape index greater than or equal to a relaxed threshold and contain voxels with a shape index greater than or equal to a high threshold. The voxels in this spherical region define the foreground seeds for the graph cut segmentation.

To produce the background seeds, the foreground region is enlarged based on the distance transform [16]. The initial background region can be obtained by inverting the enlarged foreground region. Here, the foreground region is enlarged to ensure that the background seeds do not cover the nodule to be segmented. Fig.3 shows an example of the segmented vascular nodule using the above automatic calculation of foreground and background seeds, where, the high threshold and relaxed threshold for hysteresis thresholding were chosen to be 0.92 and 0.82 respectively; and the initial foreground (Fig.4 (a2 and b2)) was enlarged 10 layers based on the distance transform to obtain the background (Fig.4(a3 and b3)).

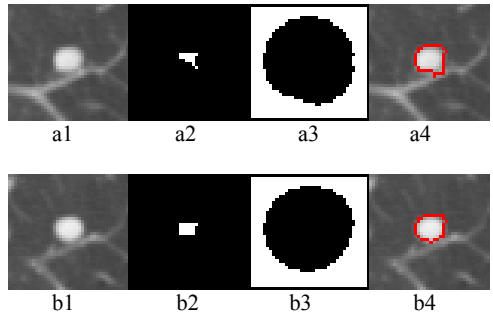

Fig.3. An example of one attached solid nodule segmentation based on the automatic calculation of initial foreground and background. (a1-b1) 3D nodule in 2 continuous slices in CT; (a2-b2) initial foreground based on high spherical concentration; (a3-b3) initial background; (a4-b4) segmentation results by the proposed graph cut based method.

3.2 Energy function

The lesion segmentation problem is formulated as a binary labeling problem, so the goal is to assign a unique label $l_i \in \{0,1\}$ to each super-pixel (mode) (where 0 is background and 1 stands for foreground (lesion)) by minimizing a Gibbs energy *E(L)* [17]:

$$E(L) = \sum_{i \in V} E_1(l_i) + \lambda \sum_{(i,j) \in \varepsilon} E_2(l_i, l_j) \quad \textbf{(4)}$$

where $E_1(l_i)$ is the data energy, determining the energy to assign the label l_i to the mode *i*, and $E_2(l_i, l_j)$ is the smoothing energy, denoting the cost of assigning the labels l_i and l_j to adjacent super-pixels *i* and *j*. λ is a weighting factor. The details of energy minimization via the graph cut algorithm for binary labeling can be found in [1]. Below we focus on how to define the two energy terms.

Data energy (t-link energy): Given the initial foreground $\{M_m^F\}$ and background regions $\{M_n^B\}$ which are automatically calculated based on the hysteresis thresholding of shape index map discussed in the section 3.1. Here, *m* and *n* are the super-pixel indices for initial foreground and background, respectively. For each super-pixel *i*, the intensity distance of the super-pixel to the foreground super-pixels $\{M_m^F\}$, weighted by the shape feature, is calculated as:

$$d_i^F = \min_m \left\| I_{\mathrm{mode}}(i) - M_m^F \right\| \times \left(1 - \exp\left(- \frac{(SI_{\mathrm{mode}}(i) - 1.0)^2}{\sigma_a^2} \right) \right),$$

where $\sigma_a = 0.3$, $I_{\mathrm{mode}}(i)$ and $SI_{\mathrm{mode}}(i)$ are the i*th* super-pixel's intensity and shape index resulting from mean shift clustering. Alternatively, an exponential function can

also be used for the calculation of the intensity similarity. The intensity distance to the background super-pixels $\{M_n^B\}$ is as: $d_i^B = \min_n \|I_{\text{mode}}(i) - M_n^B\|$. Therefore, $E_1(l_i)$ is defined as:

$$E_1(l_i = 1) = \frac{d_i^F}{d_i^F + d_i^B} \qquad E_1(l_i = 0) = \frac{d_i^B}{d_i^F + d_i^B} \tag{5}$$

We note that a nodule is generally either spherical or has local spherical elements (we define *spherical elements* as a local grouping of voxels recognized by high volumetric shape index values). It can be seen that d_i^F in Equation (5) encourages a super-pixel to have the same label as the initial foreground super-pixels if it has a similar intensity to the foreground super-pixels and also a shape feature closer to one.

Smooth energy with shape feature (l-link): The second term $E_2(l_i, l_j)$ in Equation (4) is defined as:

$$E_2(l_i, l_j) = w_{si}(E_I + E_{SI}) + (1 - w_{si}) \cdot E_I \cdot E_{SI} \tag{6}$$

where E_I is the intensity energy term, denoting the intensity difference between two adjacent super-pixels *i* and *j*, which is defined as: $E_I(l_i, l_j) = 1/(\|I_{\text{mode}}(i) - I_{\text{mode}}(j)\| + 1)$. This means super-pixels with similar intensities have a larger E_I, which leads to assigning the same labels to the two super-pixels.

E_{SI} is the shape energy term, denoting the shape difference between two adjacent super-pixels, which is defined as $E_{SI}(l_i, l_j) = 1/(\|SI_{\text{mode}}(i) - SI_{\text{mode}}(j)\| + 1)$. Similar to the intensity term, the shape energy term captures the shape features for the two adjacent super-pixels, if both the shape index values are similar, E_{SI} is larger, which means with high probability, both super-pixels have the same label. It is noted that, both the intensity mode value and shape mode value have been normalized to the same scale for the calculation of intensity energy term and shape energy term.

It can be seen from Equation (6), the intensity term and shape term are combined through a weighting function w_{si} which is defined as:

$$w_{si}(SI_{\text{mode}}(i), SI_{\text{mode}}(j)) = \exp\left(-\left(\frac{SI_{\text{mode}}(i) - SI_{\text{mode}}(j)}{\sigma_{si}}\right)^2\right), \text{ here } \sigma_{si} = 0.3$$

It is noted that, when the shapes between two adjacent super-pixels are the same, $w_{si} = 1$, and the energy depends on the first term of Equation (6). However, when two adjacent super-pixels have very different shapes, w_{si} is small, so the Equation 6 depends on the second term. Fig.4 shows a juxta-vascular nodule segmentation by using different smooth energy functions. Due to PVE in CT imaging, part of the nodule's pixels (e.g. Fig.4(a3)) have relatively low intensities, compared to that on the other slices. By using the first term only in Equation (6), those pixels with low intensity (but similar shape feature) can still be correctly identified as being part of the nodule object as seen in Fig.4 (b3). However, some small amounts of vessel (similar intensity but different shape feature) are also included into the nodule object, as seen in Fig. 4(b1-b3). This is because the first term equally considers the similarity for both of the intensity and shape features. Fig.4(c1-c3) are the results by using the second term only. It can be seen that, the shape feature is only used as a weighting to

the intensity feature. Different shapes gives lower weighting to intensity term, this is why part of nodule can be properly separately from the adjoining vessel with similar intensity, as shown in Fig.4(c1-c2). However, the pixels with lower intensity due to PVE are wrongly identified as background due to the different intensities, compared to that on the other slices, as shown in Fig.4(c3). Fig. 4(d1-d3) are the results by combining both of terms as in Equation (6), in which the nodule boundary can be properly delineated despite the PVE and the presence of vessels with similar intensity.

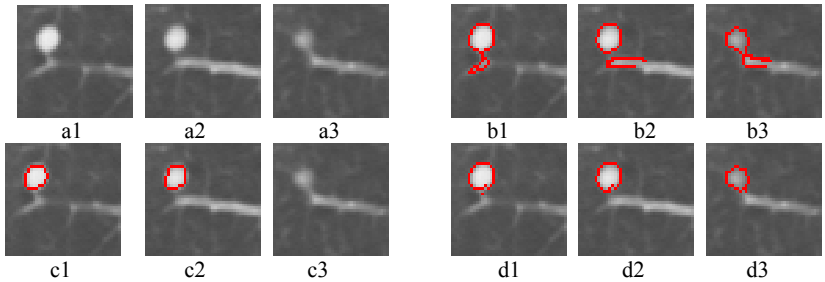

Fig.4. An example of one attached solid nodule segmentation by using different smooth energy function. (a1-a3) 3D nodule in 3 continuous slices in CT; (b1-b3) nodule segmentation by using the first term only in Equation 6; (c1-c3) results by using the second term only in Equation 6; (d1-d3) nodule segmentation by using the smooth energy in Equation 6.

4 Experimental Results and Discussion

The proposed algorithm has been evaluated on CT lung data. The three kernel window sizes (spatial h_s , intensity h_r and shape index h_{si}) in the five-dimensional mean shift clustering were set to be 3.0, 6.5 and 3.0, respectively. The proposed graph cut algorithm was applied to the mean-shift super-pixels using Equations 4, 5, and 6, where the weighting factor λ was set to be 100.

Fig.5 shows an example of the proposed method on one Ground-Glass Opacity (GGO) nodule. It is known that GGO nodules are usually with faint contrast, irregular shape and fuzzy margins, it is challenging to properly segment the nodule boundary. The proposed method demonstrates good performance on this GGO nodule segmentation. For comparison, the segmentation results without the shape feature are given in Fig. 5(a3) and (b3), where, four-dimensional mean shift with spatial and intensity features were used, also in the definition of smooth energy term (6), only the intensity energy term was considered. It can be seen that, by considering the shape index feature in both the mean shift clustering and the definition of energy formulation for graph cut, the nodule boundary can be properly delineated from the background despite the presence of other non-target structures (such as vessels).

The performance of our mode-based (mode map) graph cut algorithm was also compared with that of pixel-based method, where, in the graph construction, each vertex represents one pixel. Fig.6 shows the comparison results on another GGO nodule image, where, 46195 vertices (pixels) was constructed in the pixel-based graph, compared to 946 vertices for the super-pixel based method. Testing was performed on a system with a 2.39GHz CPU and 2GB memory. Construction of the

graph and energy minimization required 16 seconds for the pixel-based method, and 1.2 seconds for the super-pixel based method (including the mean shift). The majority of the computation time is in the graph construction, which includes the calculation of the both energy terms for each vertex. On the super-pixel based graph, the fewer vertices results in a much faster run-time.

Since the intensity mode map from the five-dimensional joint spatial-intensity-shape index mean shift algorithm expresses the local structure of the data, it can be seen that our proposed super-pixel-based method produces better results and improves the speed significantly.

For a quantitative evaluation, the proposed method has been tested on a database of clinical chest CT scans, containing 100 nodules (solid and mixed-sold nodules) with a slice thickness ranging from 0.5mm to 2.0mm. The size of the nodules ranged between 5mm to 20mm in diameter. To produce the ground truth, each nodule boundary was manually delineated by experienced radiologists. An overlap ratio between the segmented nodule and the ground truth annotation is calculated. Fig. 7 shows the overlap ratios based on the proposed method with and without shape index feature. It is noted that, without shape features, the mean overlap ratio for the whole dataset is 74% with standard deviation (*std*) of 0.08. However, the mean overlap ratio has been increased to 81% with the *std* decreasing to 0.047 by using the proposed method. This indicates the segmentation based on our proposed method is stable and accurate for different types nodules.

In this paper, the parameters for three kernel window size (spatial h_s , intensity h_r and shape index h_{si}) in Equation 2 and the weighting factor (λ) in Equation 4 are chosen experimentally. As it is noted that, kernel window sizes depend on the data structure. To improve the performance, we are currently analyzing the sensitivity of the segmentation results to those parameters and also a variable window size needs to be further investigated.

Generally speaking, it is challenging to segment GGO boundary due to its irregular shape and faint contrast. In this section, Fig.5 and Fig.6 show good examples of GGO nodule segmentation by using the proposed method. This is because, firstly, the method clusters pixels under mean shift framework by taking into account the joint spatial-intensity-shape feature. The resulting mode map significantly reduces the variance of both of the intensity and shape features. Then, the super-pixels from mean shift clustering are further merged by using graph cut algorithm. However, this is a pilot study for the GGO nodule segmentation. Further experiments (e.g. quantitative evaluation) are needed before the method can be applied in clinical practice.

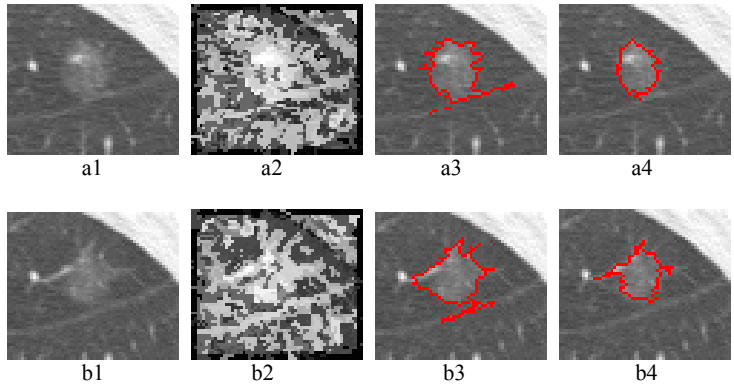

Fig.5. Example of one GGO nodule segmentation. (a1-b1): 3D GGO in two continuous slices; (a2-b2): shape index mode map from five-dimensional mean shift; (a3-b3): segmentation without shape feature; (a4-b4): segmentation results based on the proposed method.

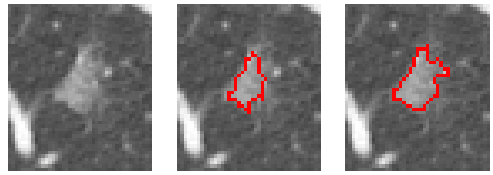

Fig.6. Segmentation result on one GGO (left) based on pixel-based graph-cut algorithm (middle) and our proposed mode-based graph-cut algorithm (right).

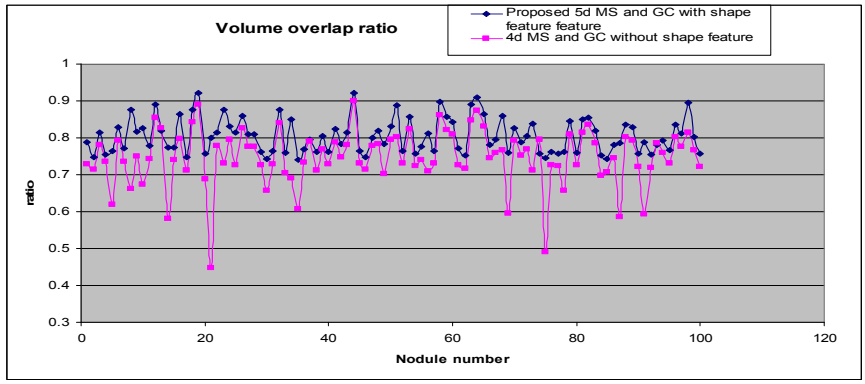

Fig.7. Volume overlap ratio based on the two different methods

5 Conclusion

We have presented a new automatic method of extracting lung nodules from CT data. A five dimensional JSIS mean shift clustering is firstly used to produce both of intensity and shape index mode maps. A graph cut algorithm is then applied to the mode map using a novel energy formulation which considers not only image intensity but also the shape feature. The joint JSIS feature provides rich information for lesion segmentation. Both by visual inspection on both solid nodules (such as Fig.3 and 4) and GGO nodules (such as Fig.5 and 6), as well as using a quantitative evaluation on 100 nodules (solid and mixed-solid) demonstrates the potential of the proposed method. The method can not only successfully segment nodules adjacent to structures of similar intensity but different shape, but also can correctly identify some part of nodules with different intensity (due to PVE in CT imaging) but similar shape.

References

1. S.A.Hijjatoleslami and J.Kitter, "Region growing: A new approach," IEEE Trans. Image Process., vol.7, no.7, pp.1079-1084, (1998).
2. W.J.Kostis, A.P.Reeves, D.F.Yankelevitz, and C.I.Henschke, "Three–dimensional segmentation and growth-rate estimation of small pulmonary nodules in helical CT images", IEEE Trans. Med. Imag., vol.22, no.10, pp.1259-1274, (2003).
3. W.Mullally, M. Betke, J.Wang, and J.P.Ko, "Segmentation of nodules on chest computed tomography for growth assessment," Med. Phys., vol.31, no.4, pp.839-848, (2004).
4. Y.Boykov, O.Veksler, R.Zabin, "Fast Approximate Energy Minimization via Graph Cuts", IEEE Trans. Pattern Analysis and Machine Intelligence, vol.23, No.11, (2001).
5.Y.Zheng, K.Steiner, T.Bauer, J.Yu, D.Shen, "Lung nodule Growth Analysis from 3D CT Data with a Coupled Segmentation and Registration Framework", ICCV, (2007).
6. Y. Li, J.Sun, C.-K.Tang and H.-Y.Shum. "Lazy snapping", ACM Trans. Graphics 23(3):303-308, (2004).
7. G.G.Slabaugh and G.B.Unal. Graph cuts segmentation using an elliptical shape prior. In ICIP(2), pp.1222-1225, (2005).
8. N.Xu, N.Ahuja, R.Bansal, "Object segmentation using graph cuts based active contours", Computer Vision and Image Understanding, 107, pp.210-224, (2007).
9. Y.Zheng, C.Kambhamettu, T.Bauer and K.Steiner, "Estimation of Ground-Glass Opacity Measurement in CT Lung Images", MICCAI, pp.238-245, (2008).
10. X.Liu, O.Veksler and J.Samarabandu, "Graph Cut with Ordering Constraints on Labels and its Applications", CPVR, Alaska, (2008).
11. O.Monga and S. Benayoun, "Using partial derivatives of 3D images to extract typical surface features," Computer Vision and Image Understanding, vol.61, pp.171-189, (1995).
12. O.Faugeras, "Three-dimensional computer vision: A geometric view-point", Cambridge, MA: MIT press, (1993).
13. H.Yoshida and J. Nappi, "Three-dimensional computer-aided diagnosis scheme for detection of colonic polyps," IEEE Trans. Medical Imaging, 20(12), pp.1261-1273, (2001).
14. D.Comaniciu and P.Meer, "Mean shift: A robust approach toward feature space analysis," IEEE Trans. on Pattern Analysis and Machine Intelligence, vol.24, pp.603-619, (2002).
15. X.Ye, X.Lin, J.Dehmeshki, G.Slabaugh, G.Beddoe, "Shape-based computer-aided detection of lung nodules in thoracic CT images," IEEE Trans. Bio-medical engineering, 56(7), 1810-20, (2009).
16. R.C, Gonzalez and R.E. Woods, Digital Image Processing, Addison Wesley, (2002).
17.S.Geman and D.Geman, "Stochastic relaxation, gibbs distributions, and the bayesian restoration of images." Trans. Pattern Analysis and Machine Intelligence, 6:721-741 (1984).